Journal of Engineering and Technological Sciences

Research Paper

Synthesis of Geopolymer from Ferronickel Aluminosilicate Waste

Tjokorde Walmiki Samadhi*, Winny Wulandari, Aya Anisa Dwinidasari, & Arum Rahmasari

Faculty of Industrial Technology, Institut Teknologi Bandung, Labtek X Building,
Jalan Ganesa 10 Bandung 40132, Indonesia

*Corresponding author: twsamadhi@itb.ac.id

Abstract

The nickel industry in Indonesia generates massive volumes of ferronickel slag that may harm the environment. This research evaluates the feasibility of utilizing coal fly ash and slag from a ferronickel smelter in Obi Island in Indonesia to synthesize geopolymer, an environmentally friendly cementitious material. Compressive strength of geopolymer mortars was measured as a function of slag particle size (coarse and fine), fly ash mass fraction in the dry aluminosilicate binder precursor blends (0.4 and 0.8), and thermal curing period (24 and 48 hours). Mortar specimens were produced by mixing ash and slag with activator solution and sand. The activator solution contained Na_2SiO_3 and NaOH at a mass ratio of 2:1. Solid reactants to activator solution mass ratio was 3.33. After heat curing, specimens were held in ambient conditions to an age of 7 days. The compressive strength of the mortars was in the 2.1-24.8 MPa range. Geopolymer mortars were able to comply to Indonesian SNI 15-2049-2004 or US ASTM C1329-05 standards for Portland cement. FTIR and XRD characterizations confirmed the conversion of fly ash and slag into amorphous geopolymers at near ambient temperature. Finer slag particle size increased reactivity, ultimately producing higher compressive strength.

Keywords: *aluminosilicate; ash; cement; ferronickel; geopolymer; slag; valorization; waste.*

Introduction

According to current estimation, Indonesia is ranked as having the largest nickel reserves in the world at 55 million tons. The highest nickel production rate in Indonesia was 1 million ton/year in 2021 (U.S. Geological Survey, 2024). The ferronickel production process consists of nickel ore size reduction and drying, calcination, and smelting operation which includes calcined ore (or calcine) reduction, melting and refining (Coelho et al., 2024). The calcine reduction step generates a large volume of ferronickel slag (FS), which is a mixture of metal oxides with little or negligible economical value. Depending upon the smelting process, FS could be further categorized as electric arc furnace slag (EFS) and blast furnace slag (BFS). Major oxide components of EFS are SiO_2 (40-60 %-wt), MgO (20-40 %-wt), and Fe_2O_3 (approximately 10 %-wt). On the other hand, major components of BFS are CaO (25-35 %-wt), SiO_2 (25-35 %-wt), Al_2O_3 (15-25 %-wt), MgO (7.5-12.5 %-wt), and Fe_2O_3 (approximately 2.0 %-wt) (Han et al., 2023).

Indonesia produced 4 million tons of FS in 2019 (Edwin et al., 2019). Disposal of large volumes of slag in landfills is associated with the risk of heavy metal leaching that may harm the environment (Yanning et al., 2024). With the current positioning of nickel as the premiere metallic mineral product of Indonesia and national development towards downstream nickel processing, FS accumulation can be projected to be a significant environmental issue in the near future. Various utilization pathways for FS have been explored. These include fine and coarse aggregates for concrete and asphalt pavement, raw materials for cement production, production of magnesium and ferroalloys, ceramic tile manufacture, and as raw materials for geopolymers (Coelho et al., 2024; Han et al., 2023; Kuri, et al., 2021a; Shang et al., 2021; Wang et al., 2023; Zulhan & Agustina, 2021).

Geopolymers refer to aluminosilicate polymeric materials that were developed beginning in the late 1970s. Geopolymers are traditionally produced by reacting aluminosilicate solids with concentrated activator solution containing alkali (K, Na, Ca, etc.) hydroxide and/or alkali silicates. Steps involved in alkali-activated geopolymer synthesis

ISSN: 2337-5779
J. Eng. Technol. Sci. Vol. 57, No. 4, 2025, 431-444
DOI: 10.5614/j.eng.technol.sci.2025.57.4.1

include chemical attack of the silicate structure of aluminosilicate solids by the alkali solution, forming several classes of Si-O-Al structures. These structures include poly(sialate) (-Si-O-Al-O-), poly(sialate-siloxo) (-Si-O-Al-O-Si-O-), and poly(sialate-disiloxo) (-Si-O-Al-O-Si-O-Si-O-). These soluble aluminosilicate complexes then diffuse into inter-particle voids. Reaction of these complexes with alkali silicates in the activator solution forms amorphous N-A-S-H (sodium aluminate silicate hydrate), C-A-S-H (calcium aluminate silicate hydrate), and/or N-C-A-S-H (sodium calcium aluminate silicate hydrate) gel phases, depending on the chemical composition of the aluminosilicate precursors and activator solutions. These gel phases contain three-dimensional randomly oriented alkali silicate chains that gradually harden through condensation and crosslinking reactions. The network of negatively charged alkali silicate chains is electrostatically balanced by alkali cations supplied by the activator solution (Chuewangkam et al., 2024; Ng et al., 2018).

Within approximately the last 10 years, acid activation has also been studied as an alternative geopolymer synthesis route that promises higher strength and environmental durability (Tchakouté & Rüscher, 2017). Acid-activated geopolymers (also known as SAP or silico-alumino-phosphate geopolymers) are typically prepared using phosphoric acid and phosphate salts such as KH_2PO_4 and $Al(H_2PO_4)_3$. In the acid activation route, the low pH environment disrupts SiO_2 and AlO_4 units in the aluminosilicate solid precursors, forming units containing -Al-O-P-, -P-O-Si-O-P-O-, -Si-O-Al-O-P-, and -Si-O-Si-O- groups. Collectively, these groups then undergo polycondensation, forming silicate aluminum phospate network. The coordination number of Al cations may interchange between 4 to 6, thereby conserving the electrostatic charge neutrality of the geopolymer product without the need for alkali cations from the activator solution (Wu et al., 2024). The compressive strength of alkali-activated geopolymer mortars based on ground granulated blast furnace slag (GGBS) was reported in the 40-75 MPa range after 28 days curing (Mishra et al., 2024). In comparison, acid-activated ferronickel slag geopolymer mortars exhibited compressive strengths in the 1.0-12 MPa range (Li et al., 2022). In the form of concrete, geopolymers also generally exhibit higher durability against freeze-thaw cycle and sulfate attack compared to ordinary Portland cement (OPC) concrete (Tao et al., 2025).

Geopolymerization reactions may occur at or near ambient temperatures, thus avoiding the fuel combustion necessary in Portland cement production. Aluminosilicate raw materials for geopolymer production include a wide range of non-waste and waste materials. Non-waste materials include metakaolin or calcined kaolin, clays, and lateritic soils (Kaze et al., 2022; Lekshmi et al., 2023). Various waste materials, such as metallurgical slag, coal fly ash, biomass ash, mining tailing, waste firebrick, construction demolition waste, and more may be used as aluminosilicate precursors in geopolymer production (Bewa et al., 2020; Detphan & Chindaprasirt, 2009; Kaze et al., 2024; Tian et al., 2022; Vásquez et al., 2016). McLellan et al. (2011) estimated a greenhouse gas (GHG) emissions reduction of 44-64% compared to Portland cement-based concrete, based on available prospective geopolymer raw materials in Australia. Carreño-Gallardo et al. (2018) reported an estimated global carbon emission reduction potential of more than 1400 million tons of CO_2-equivalent per year of Portland cement (OPC) substitution by dry-mix geopolymer manufactured from silica-rich sand and sodium carbonate. Life cycle assessment of OPC versus geopolymer-based concrete reported by Gomes et al. (2019) suggested that geopolymer concrete potentially emits 43% less carbon emission. With these characteristics, geopolymer is regarded as an environmentally attractive Portland cement substitute.

FS utilization as geopolymer aluminosilicate precursor is quite promising. In this role, FS may substitute other aluminosilicates in geopolymer production by as much as 30%. This substitution level is higher compared to FS utilization as supplementary cementitous materials (SCM) in OPC product blending, which is limited to 20% (Yanning et al., 2024). On the other hand, literature data point to the rather wide range of oxide composition variations exhibited by FS. This variability in FS oxide composition is accompanied by a nearly twofold variation in compressive strength as reviewed by Mishra et al. (2024).

The current research explored the preliminary technical feasibility of geopolymer preparation from solid wastes generated by a ferronickel plant in Obi Island in eastern Indonesia. Inherent compositional variations in mineral-based materials imply that feasibility and proper conditions for geopolymerization must be determined on a case-by-case basis. Proving this feasibility is critical to alleviate the FS accumulation on the island site to produce less environmentally impactful engineering materials for use on the smelter premises and on the surrounding island. Due to the preliminary nature of this study, emphasis was given on confirming the amenability of Obi Island ferronickel slag to geopolymerization as indicated by product mechanical strength against industrial standards, and structural evidence of geopolymerization. Insights on opportunities and technical challenges of ferronickel slag reuse via geopolymerization shall also be useful in developing sustainable processing in other smelters elsewhere in the country.

DOI: 10.5614/j.eng.technol.sci.2025.57.4.1

Data and Methodology

Ferronickel slag (FS) was obtained from a ferronickel smelter facility operated by Harita Nickel group in Obi Island in North Maluku Province. Coal fly ash (FA) was sourced from a nearby power plant operated by the same corporation. To prepare the FS for geopolymerization, 1 kg of as-received specimen was ground in a 3-liter ceramic ball mill jar for 120 minutes using mullite grinding balls, followed by particle size distribution (PSD) measurement by standard sieve analysis. Elemental compositions of these raw materials were measured by X-ray fluorescence (XRF).

Analytical grade NaOH solid flakes and technical grade $Na_2SiO_3 \cdot 6H2O$ were obtained from local chemical suppliers in Bandung. To produce geopolymer mortar specimens, Ottawa-type graded silica sand with particle size distribution according to ASTM C778-06 was obtained from the Civil Engineering Department at Institut Teknologi Bandung. NaOH flakes were dissolved in demineralized water to prepare a stock of 10.0 M NaOH solution, which is close to the optimum concentration reported in the literature (Samantasinghar & Singh, 2019).

In the preliminary experiment, a series of qualitative checks were undertaken to identify the proper aluminosilicate precursors and the activator solution mass ratio (S/L) and sodium silicate to hydroxide (S/H) mass ratio in the activator solution. To produce geopolymer paste specimens, FA and FS specimens were mixed by a planetary mixer at 50 rpm for 3 minutes. The activator solution was then added and mixed for 3-4 minutes until a smooth paste was obtained. Small disks of geopolymer paste specimens were cast in reused polyethylene drinking cups and were allowed to harden at ambient conditions for 24 hours. Since the amount of FS specimen received from the Obi Island facility was limited due to logistical constraints, this small-scale approach in the preliminary experiment was selected over industrial standard methods such as the flow table test (ASTM C230).

In the main experiment, geopolymer mortar specimens were prepared by dry mixing ash–slag precursor blends in the planetary mixer at 50 rpm for 3 minutes. The activator solution, optimized for the best S/L and S/H values from preliminary experiments, was then added, followed by an additional 5 minutes of mixing. The standard sand was then added and further mixed for 7 minutes. The mortars were then poured into 50×50×50 mm steel mold and compacted to remove trapped air bubbles. The cast mortar specimens were then loosely covered by a plastic sheet and moved to an electric oven for thermal curing for a prescribed period. Afterwards, the specimens were removed from the oven and kept loosely covered such that the specimens reach 7-day age before submission for tests. Specimen characterizations included compressive strength measurement using a universal uniaxial load tester, identification of chemical bonds by FTIR (Shimadzu Prestige 21, Analytical Chemistry Laboratory, Institut Teknologi Bandung), solid phases development by XRD (Bruker D8, Department of Chemical Engineering, Institut Teknologi Bandung), and microstructural characterization by SEM (Hitachi SU3500, Research Center for Nanoscience and Nanotechnology, Institut Teknologi Bandung). Experimental variables were FS particle size cuts, FA mass fraction in the dry aluminosilicate precursor, and mortar thermal curing period at 60 °C. Sand to geopolymer binder mass ratio was kept at 2.75 in all runs. The experiment was undertaken using a 2^3 full factorial statistical experimental design, which included three replicates of the centerpoint run.

Results

Raw Materials Preparation and Characterization

Visual appearance of the FS and FA specimens are presented in Figure 1. Figures 2a and 2b present the particle morphology of ground FS and as-received FA, respectively. Sieve analysis results of ground FS and as-received FA are tabulated in Table 1, while Figure 3 presents the data as cumulative particle size distributions. The FA is finer than the ground FS, with an estimated cumulative mass fraction less than 80% (D_{80}) values of 80 μm for FA compared to 500 μm for ground FS. A key question at this preliminary developmental stage is the particle size at which substantial geopolymerization starts to occur. For this, the ground FS was classified into three size fractions, namely coarse (-100/+200 mesh), medium (-200/+325 mesh), and fine (-325/+800 mesh). The approximate midrange particle sizes of these fractions were 112, 60, and 30 μm, respectively.

Figure 1 Visual appearance of (a) FS and (b) FA specimens from Obi Island ferronickel plant.

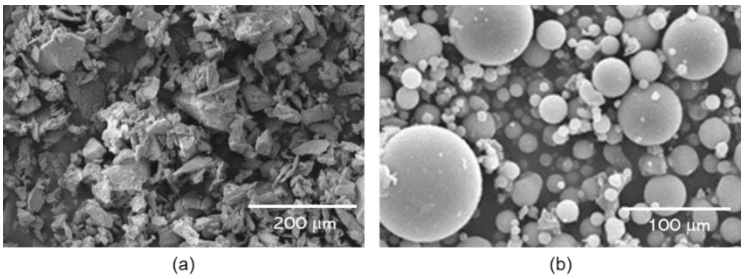

Figure 2 Particle morphology of (a) ground FS and (b) as-received FA specimens.

Table 1 Notations and levels of ZnO biosynthesis experimental variables.

Mesh no.	Particle size, µm	Cumulative %-mass finer	
		Slag (ground)	Fly ash (as received)
800	15	0.0%	0.7%
325	44	1.9 %	24.2%
200	74	6.6 %	76.6%
100	149	15.1 %	85.4%
50	297	42.6 %	97.3%
30	595	94.2 %	99.3%
16	1190	100.0 %	100.0%

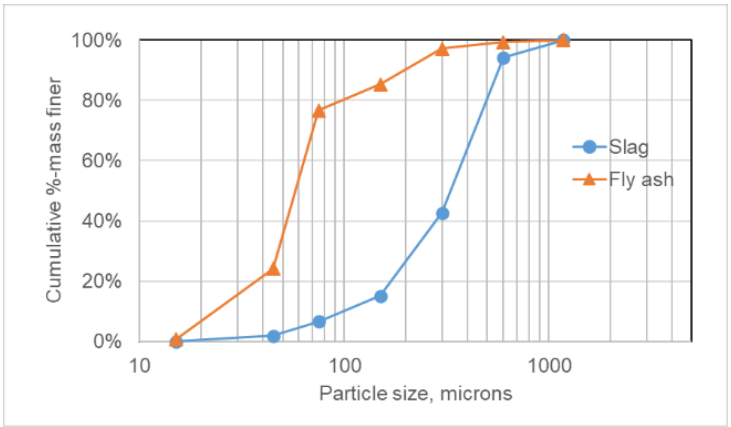

Figure 3 Cumulative particle size distribution curves of ground FS and as-received FA determined by standard sieve analysis.

The elemental compositions of each slag size fractions were analyzed by XRF, the results of which are summarized in Table 2. Elemental compositions of the three particle size fractions are nearly identical, indicating that the elements are homogeneously distributed throughout the slag and that no specific mineral phase liberation occurred due to the grinding. Thus, the effect of slag particle size can be concluded to be independent of the slag composition. The table also contains compositions of fly ash – slag blends used in the main experiment and Si/Al molar ratios of the fly ash, different size fractions of the slag, and the fly ash – slag blends.

DOI: 10.5614/j.eng.technol.sci.2025.57.4.1

The total mass percentage of SiO_2, Al_2O_3, and Fe_2O_3 of the fly ash is approximately 73%, indicating that it belongs to the ASTM Class F FA ($SiO_2 + Al_2O_3 + Fe_2O_3 > 50\%$, and $CaO \leq 18\%$) (ASTM, 2019). Class F FA generally exhibits higher reactivity compared to Class C FA, resulting in higher mechanical strength particularly when the specimen curing involves heating at mild temperatures (Kaya et al., 2020; Wardhono, 2018). Based on the elemental composition analysis, the Obi Island smelter FS specimen is classified as high-magnesium nickel slag (HMNS). It is notable that most of the recent published literature on the geopolymerization of HMNS employed blends of HMNS and other aluminosilicate precursors such as blast furnace slag, coal fly ash, and municipal waste incineration ash (Bouaissi et al., 2019; Cao et al., 2018; Kuri, et al., 2021a; Long et al., 2021; Yang et al., 2017). Reasons for blending HMNS with FA include the higher reactivity of FA to chemical attack by the activator solution, and to ensure that the Si/Al molar ratio of the reacting mixture is within its optimum range (Kuri, et al., 2021b; Li et al., 2022).

Table 2 Elemental analysis results of classified, ground FS and as-received FA

Element	Compositions (%-mass)								
	Coal fly ash (FA)	Ferronickel slag			Fly ash / slag blends				
		Coarse (CS) -100/+200 mesh Midrange: 112 μm	Medium (MS) -200/+325 mesh Midrange: 60 μm	Fine (FS) -325 mesh Midrange: 30 μm	FA:CS = 0.4	FA:FS = 0.4	FA:CS = 0.8	FA:FS = 0.8	FA:MS = 0.6
Si	18.010	23.290	23.120	23.050	21.178	21.034	19.066	19.018	20.054
Al	10.260	2.540	2.500	2.960	5.628	5.880	8.716	8.800	7.156
Fe	10.440	4.550	4.450	4.310	6.906	6.762	9.262	9.214	8.044
Ca	5.450	0.435	0.431	0.480	2.441	2.468	4.447	4.456	3.442
Mg	4.050	21.540	21.670	21.140	14.544	14.304	7.548	7.468	11.098
S	1.160	0.026	0.027	0.057	0.479	0.498	0.933	0.939	0.707
Na	0.655	0.041	0.041	0.058	0.287	0.297	0.532	0.536	0.409
K	0.701	0.108	0.094	0.119	0.345	0.352	0.582	0.585	0.458
Ti	0.487	0.045	0.044	0.048	0.222	0.224	0.399	0.399	0.310
Mn	0.118	0.440	0.433	0.409	0.311	0.293	0.182	0.176	0.244
P	0.054	0.000	0.000	0.000	0.022	0.022	0.043	0.043	0.033
Ba	0.081	0.000	0.000	0.000	0.032	0.032	0.065	0.065	0.048
Sr	0.057	0.000	0.000	0.000	0.023	0.023	0.046	0.046	0.034
Cr	0.020	1.080	1.070	1.010	0.656	0.614	0.232	0.218	0.440
Ni	0.018	0.016	0.016	0.017	0.017	0.018	0.018	0.018	0.017
V	0.012	0.009	0.008	0.007	0.010	0.009	0.011	0.011	0.010
Cl	0.018	0.009	0.008	0.011	0.012	0.013	0.016	0.016	0.014
Zr	0.009	0.000	0.000	0.000	0.004	0.004	0.008	0.008	0.006
Zn	0.009	0.008	0.008	0.008	0.008	0.009	0.009	0.009	0.009
Co	0.006	0.000	0.000	0.000	0.002	0.002	0.005	0.005	0.003
Si/Al	1.76	9.17	9.25	7.79	3.76	3.58	2.19	2.16	2.80

Results of phase characterization FS and FA specimens by XRD are given in Figure 4. Crystalline phases identified in the FS specimen included enstatite ($Mg_2Si_2O_6$, JCPDS number 86-0430) and forsterite (Mg_2SiO_4, JCPDS number 34-0189). The predominance of magnesium silicate phases was consistent with measured elemental composition in Table 2. The coal fired steam powerplant FA specimen contained quartz (SiO_2, JCPDS number 46-1045), mullite ($3Al_2O_3{\cdot}2SiO_2$, number JCPDS 15-776), and gypsum ($CaSO_4$, JCPDS number 01-070-0982). The latter phase originated from powerplant SOx emission control system that injects limestone slurry into the furnace stack gas, thereby reacting with SO_x forming $CaSO_4$ particulate that is harmless to the environment.

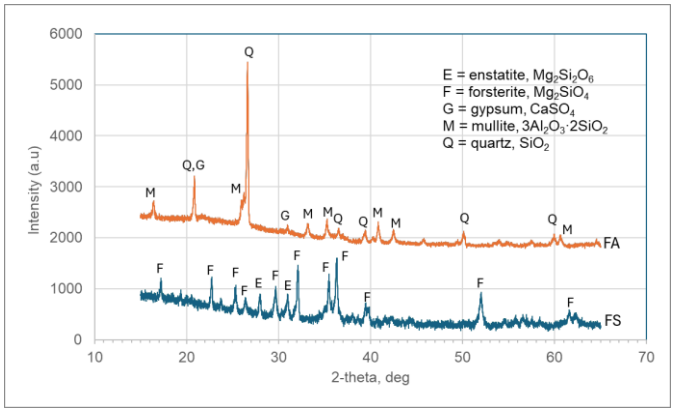

Figure 4 X-ray diffractogram of FS and FA specimens from Obi Island smelter plant (E = enstatite, F = forsterite, G = gypsum, M = mullite, Q = quartz).

Preliminary Experiment

The preliminary experiment was undertaken to identify the proper solid/liquid (S/L) ratio and alkali silicate/alkali hydroxide (Na_2SiO_3/NaOH or S/H) ratio for the mechanical integrity of the geopolymer paste. The availability of sufficient water in geopolymerization is critical in ensuring intimate mixing between the reacting components and the availability of soluble hydroxide ions responsible for the dissolution of Al^{3+} and Si^{4+} cations from the solid precursors. However, excessive liquid may lead to the formation of pores during the geopolymer curing stage (Falayi, 2019). In geopolymerization, sodium hydroxide serves as a catalyst that accelerates the dissolution of Al^{3+} and Si^{4+} from the precursors, while sodium silicate is polymerized along with the soluble silicates and aluminates produced by the dissolution of precursors, forming binder gel phase that fills the voids between unreacted particles. However, excessive amount of sodium silicate implies that the strength of the overall geopolymer product is predominated by the binder phase, which exhibits lower compressive strength compared to bonded precursor particles (Fansuri et al., 2012). These published observations imply that optimum S/L and S/H ratios exist. As such, the best values of these ratios determined in the preliminary experiment were subsequently used as fixed parameters in the main experiment.

Criteria for selection of these ratios included hardness after 24 hours (measured by hand; higher is better), geopolymer paste homogeneity and flowability (visually judged; higher is better), and liquid activator solution uptake (lower is better). Scoring weights of these criteria were calculated by the Analytical Hierarchy Process (AHP) method as 45.45, 45.45, and 9.10%, respectively. Scoring for each criterion was done on a 1 to 10 scale (1 = worst, 10 = best).

Table 3 summarizes the geopolymer paste synthesis conditions and total weighted scores of each run. The experimental runs were classified into two groups, namely for fly ash mass fractions of 0.8 and 0.4. It was anticipated that geopolymerization behavior differs substantially between these fractions. For fly ash fraction of 0.8, the best specimen was obtained at S/L of 3.3 and S/H of 2.0. The same set of ratios also produced the best specimen at fly ash fraction of 0.4.

Table 3 Weighted semi-quantitative judgment results from the preliminary experiment

Run no.	FA mass fraction*	S/L (w/w)	S/H (w/w)	Weighted score based on 3 criteria			
				A (45,45%)	B (45,45%)	C (9,10%)	Total
1	0.8	4	1	8	5.0	5.5	6.41
2	0.8	4	2	8	5.5	6	6.68
3	0.8	3.3	1	8	8.5	7	8.14
4	0.8	**3.3**	**2**	**8**	**9.0**	**7.5**	**8.41**
5	0.8	2.5	1	7	7.0	8	7.09
6	0.8	2.5	2	7	6.5	8.5	6.91
7	0.4	4	1	7	4.0	4	5.36
8	0.4	4	2	7	4.5	4.5	5.64
9	0.4	3.3	1	7	7.5	6.5	7.18
10	0.4	**3.3**	**2**	**7**	**8.0**	**7**	**7.45**
11	0.4	2.5	1	6	6.5	8	6.41
12	0.4	2.5	2	6	5.0	8.5	5.77

*) based on dry binary fly ash – ferronickel slag blends as the geopolymer aluminosilicate precursors

DOI: 10.5614/j.eng.technol.sci.2025.57.4.1

Main Experiment

Compressive Strength

Variables in the main experiment were FS particle size (X_1, expressed as the median of particle size for each FS size fraction), proportion of FA in the dry aluminosilicate precursor blend (X_2 = mass fraction of FA/(FA+FS)), and heat curing period at a constant temperature of 60 °C (X_3). Based on results of the preliminary experiment, geopolymer mortar specimens in the main experiment were prepared with S/L=3.3 and S/H=2.0. Figure 5 presents a visual example of 50×50×50 mm cube specimens prepared for the compressive strength measurement. Table 4 summarizes the compressive strength measurement results after heat curing at a prescribed duration followed by further holding at ambient conditions for a total of 7 days post-casting curing. The 7-day compressive strengths ranged from 2.1 MPa (Run #1) to 24.8 MPa (Run #8). These values are comparable to FS-based geopolymers reported in the literature, which varied in the 8-40 MPa (Kuri, et al., 2021a; Nguyen & Castel, 2023).

To assess the preliminary technical feasibility of Obi Island FS utilization for geopolymer production, measured compressive strengths are compared in Table 5 against several industrial standards. These standards are Indonesian SNI 15-2049-2004 for Portland cement specifications and US ASTM C1329-05 for mortar cement. Table 5 indicates that Run number 8 met the standards for the most types of cement, particularly for medium to high-strength masonry applications with high sulfate resistance. The centerpoint run represented the second-best condition, while Run numbers 1, 2, and 5 did not meet any industrial standard included in the table.

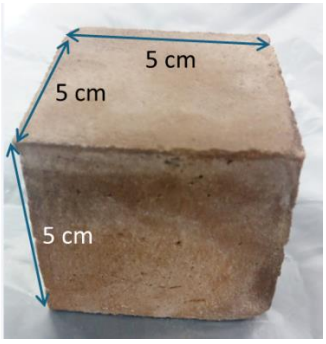

Figure 5 Visual appearance of the geopolymer mortar cube specimens after curing; the specimen shown was prepared with FA/(FA+FS) mass ratio of 0.8, fine slag particles, and a heat curing period of 48 hours.

Table 4 Compressive strength of slag-ash geopolymer mortar specimens in the main experiment after 7 days of curing.

Run No.	Variables			Si/Al	Compressive strength (MPa)
	Slag particle nominal median size (X_1, μm)*	Fly ash mass fraction (X_2)*	Curing period (X_3, hrs.)		
1	110	0.4	24	3.76	2.1
2	30	0.4	24	3.58	2.9
3	110	0.8	24	2.19	3.6
4	30	0.8	24	2.16	6.3
5	110	0.4	48	3.76	3.1
6	30	0.4	48	3.58	6.1
7	110	0.8	48	2.19	10.5
8	30	0.8	48	2.16	24.8
9	70	0.6	36	2.80	7.7
10	70	0.6	36	2.80	8.2
11	70	0.6	36	2.80	8.9

Table 5 Compliance of 7-day compressive strengths of slag-ash geopolymer mortar specimens to industrial standards

	SNI 15-2049-2004				ASTM C1329-05		
Cement type → Run no.	**I**	**II**	**IV**	**V**	**M**	**N**	**S**
1	no	no	no	no	no	no	no
2	no	no	no	no	no	no	no
3	no	no	no	no	no	yes	no
4	no	no	no	no	no	yes	no
5	no	no	no	no	no	no	no
6	no	no	no	no	no	yes	no
7	no	no	yes	no	no	yes	yes
8	yes	yes	yes	yes	yes	yes	yes
9-11 (averaged)	no	no	yes	no	no	yes	no

An ANOVA statistical data treatment was undertaken on the measured compressive strengths in Table 4, the results of which are summarized in Table 6. Due to the relatively low number of specimens used in the experiment, the linear model in the ANOVA was limited to 2-way interactions. A confidence level of 95% was used to judge the significance of each effect. Raw and adjusted coefficients of correlation are both high, indicating a good fit of the ANOVA model to experimenta data.

P-values in Table 6 indicate that all three geopolymer synthesis variables impacted the mortar compressive strength in a statistically significant manner at 95% confidence level. Signs of the main effect regression coefficients suggested that higher compressive strength may be achieved by finer slag particles, higher proportion of fly ash, and longer heat curing period. Only one interaction was statistically significant, namely that between FA proportion in dry aluminosilicate precursor blend and heat curing period (X_2X_3). Compressive strength behaves linearly with respect to the three synthesis variables, indicated by the non-significant non-linearity term.

Table 6 Summary of ANOVA treatment results of compressive strength data

Source of variation	Regression coefficient	Sum of squares	P-value
Main effects:			
Slag particle size (X_1)	-2.60	54.08	0.034
FA proportion (X_2)	3.88	120.12	0.012
Curing t (X_3)	3.70	109.52	0.013
2-way interactions:			
X_1X_2	1.65	21.78	0.100
X_1X_3	1.72	23.80	0.091
X_2X_3	2.65	56.18	0.032
Non-linearity:		1.546	0.575
Coefficient of correlation	R^2 = 97.0%		
	R^2_{adj} = 90.2%		

Chemical Bonds, Solid Phases, and Microstructural Characterizations

Two specimens were selected for chemical bond characterization using FTIR to elucidate the effect of slag particle size on geopolymerization reactivity. Figure 6 presents FTIR spectra of geopolymer mortar specimens from Run numbers 7 and 8, respectively. Table 7 summarizes the IR absorption band identification as referenced from Rosas-Cesarez et al. (2018) and Maragkos et al. (2009). These authors reported FTIR spectra of geopolymers synthesized from coal fly ash and ferronickel slag, respectively.

Particularly pronounced IR absorption bands are observed in wavenumbers of 900-1000 cm^{-1} and 3450 cm^{-1}. Bands in the 900-1000 cm^{-1} range are attributed to the asymmetric stretching of Si-O-Si and Al-O-Si that are primary markers of the geopolymeric amorphous gel structure. The band at 3450 cm^{-1} is attributed to the stretching vibration of hydroxyl groups of the N-A-S-H (sodium aluminosilicate hydrate) gel phase. Altogether, these bands confirm the occurrence of geopolymerization in the specimens. Absorption bands in the 600-650 cm^{-1} range are attributed to crystalline quartz and mullite phases (Rosas-Casarez et al., 2018). The presence of these bands in the geopolymer specimens suggests that the geopolymerization of raw materials is not yet complete. The O-C-O stretching in the 1410-1570 cm^{-1} range is attributed to carbonate groups formed by reaction between excess alkali on the specimen external surface and carbon dioxide in the atmosphere, a phenomenon known as efflorescence. Extensive efflorescence may be detrimental for the

DOI: 10.5614/j.eng.technol.sci.2025.57.4.1

aesthetics and mechanical strength of geopolymer concrete due to alkali removal from the network structure and increased surface deterioration (Simão et al., 2021; Wang et al., 2020).

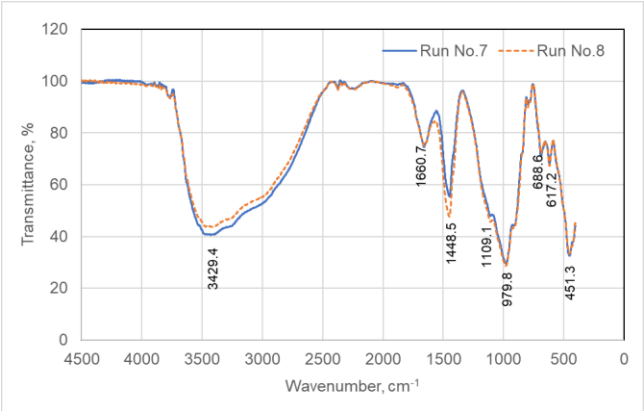

Figure 6 FTIR spectrum of geopolymer mortar specimens from Run no.7 (coarse slag, 80% fly ash, 48 hrs curing) and Run no.8 (fine slag, 80% fly ash, 48 hrs curing).

Table 7 Identification of IR absorption peaks.

Wavenumber (cm^{-1})	Vibrational mode	Presence in specimens			
		Run no.7	Run no.8	Fly ash	Slag
~460	O-Si-O, O-Al-O vibrations	yes	yes	yes	yes
~600-650, ~750-810	Si-O-Si, Al-O-Si symmetrical stretching	yes	yes	yes	yes
~900-1100	Si-O-Si, Al-O-Si asymmetrical stretching	yes	yes	yes	yes
~1410-1570	O-C-O stretching	yes	yes	no	no
~1650	H-O-H bending vibration	yes	yes	no	no
~3450	OH group stretching vibration	yes	yes	no	no

Figure 7 presents X-ray diffractograms of geopolymer paste (prepared without the addition of sand) prepared using ash/slag mass ratio of 0.6 and heat curing period of 24 hrs. Two diffractograms are presented in the figure, namely for geopolymer prepared using coarse and fine ferronickel slag particles. In comparison with XRD patterns of raw materials in Figures 4, the geopolymer specimens exhibit lower crystallinity which is consistent with the general observation that geopolymeric alkali-aluminosilicate gel phase is amorphous regardless of the crystal structure of its aluminosilicate precursor. Crystalline phases observed in the geopolymers include olivine and quartz, which is attributed to unreacted coal fly ash and ferronickel slag particles. As the FS particle size is reduced (top diffractogram in Figure 7) its reactivity increases as indicated by the smaller number of olivine and quartz peaks present. Decreasing presence of remaining crystalline phases originating from raw materials, and the absence of new crystalline phases in geopolymers are also reported in the literature (Li et al., 2012).

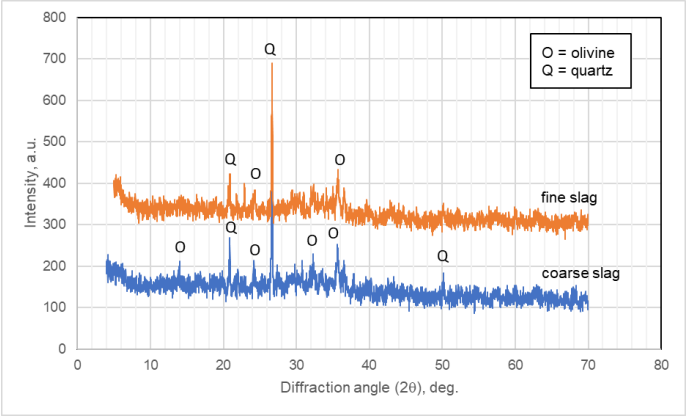

Figure 7 X-ray diffractograms of geopolymer paste specimens at ash/slag mass ratio of 0.6 and heat curing period of 24 h.

The effect of FS particle size on the geopolymer mortar microstructure is described in Figures 8a (coarse FS), 8b (medium FS), and 8c (fine FS). Figure 8a suggests a poor bonding between the geopolymer gel phase and unreacted solid particles. The surface of this specimen is characteristically rough, with loosely bonded raw material particles (indicated by white boxes in the figure) creating open pores and cracks. The medium FS specimen (Figure 8b) indicates a much less prevalence of loosely bonded particles and large surface cracks and pores. This is in accordance with compressive strength data in Tables 4 and 5, which indicate that reasonable levels of reactivity against the activator solution and the concurrent development of compressive strength started to appear at medium FS size fraction. When the FS size fraction was reduced further (Figure 8c), the geopolymerization reactivity increased further so that no loosely bonded particle was observed on the specimen surface. Specimens prepared using medium and fine FS exhibited the formation of needle-shaped crystalline phase. Comparison similar microstructural features reported in the literature identify the needle-shaped phase as ettringite. This phase has been observed in the intial setting phase of FA-slag based geopolymers (Samantasinghar & Singh, 2019).

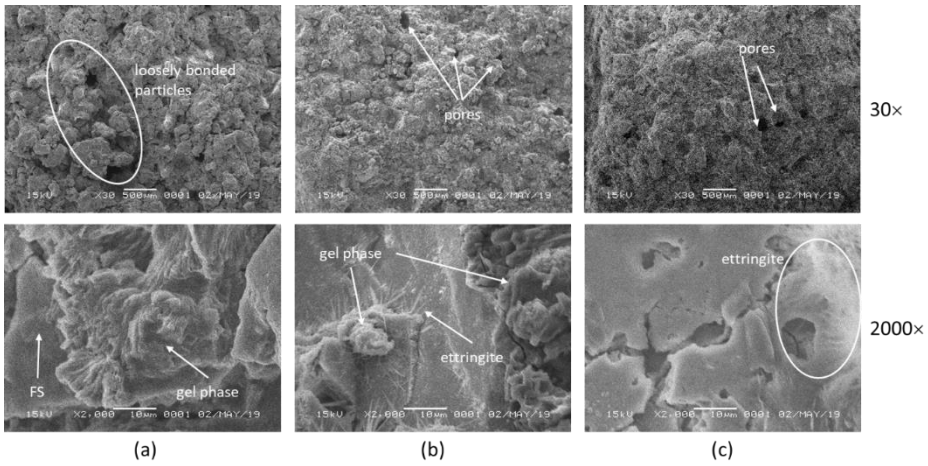

Figure 8 SEM images of geopolymer mortar specimens using coarse (Run no.1), medium (Run no.11), and fine (Run no.8) FS particle sizes (at 30× and 2000× magnifications).

Discussions

It is interesting to compare optimum S/L and S/H ratios determined from the preliminary experiment to values reported in the literature. Compressive strength of fly ash – GGBFS geopolymer concrete reported by Niş (2019) suggested an interaction between NaOH solution concentration and S/H mass ratio in the activator solution. The author reported an optimum S/H of 2.0 at NaOH concentration of 10 M, in accordance with the value selected in the current work. A range of optimum S/L mass ratio values have been reported in the literature. The optimum S/L mass ratio reported by Marczyk et al. (2022) for fly ash – based geopolymer was identical to the value identified in this preliminary experiment namely 3.3. Al-Safi (2021) reported a lower optimum S/L value of 2.0 for blast furnace slag geopolymers. Xu et al. (2021) studied the effect of S/L on the strength and shrinkage of blast furnace slag geopolymer, in which S/L was varied in the 1.0-1.5 range. These authors observed the highest compressive strength at S/L = 1.5. However, it is notable that this ratio is at the high end of their range of study. As such, the optimum S/L value might be higher than 1.5.

Comparison of compressive strengths of coarse versus fine FS data pairs in the main experiment (Table 4) suggested that fine FS produced roughly twice the strength of coarse FS. Moreover, Table 5 and Figure 7 indicate that the Obi Island FS must be ground to at least the medium size fraction (with a midrange particle size of approximately 70 μm) to enable substantial geopolymerization. As a comparison in the literature, Petrakis et al. (2019) reported an increase in 7-day compressive strength from 20 to 61 MPa as the median size of the slag was reduced from 40 to 12 μm. These authors attributed the increase in reactivity to geopolymerization as due to an increase in particle specific surface area. Argument for particle size of 70 μm as a rough cutoff for FS grinding to obtain an acceptable rate of geopolymerization is also supported by the work of Mustofa and Pintowantoro (2017). Using only FS that has been ground to particle size of ≤ 70 μm, these authors obtained compressive strengths of 8-12 MPa after 28-day hardening.

Table 4 suggests that an increase in proportion of the slag from 20% to 60% decreases the 7-day compressive strength. This trend is in accordance with the observation reported by Yang et al. (2014) who observed an increase of compressive strength with HMNS proportion of 0 to 20%, followed by a decrease in strength at HMNS proportions from 20% to 60%. These authors attribute the subsequent strength decrease to the lack of Al and Ca in HMNS, which is consistent with

DOI: 10.5614/j.eng.technol.sci.2025.57.4.1

the Obi Island HMNS elemental analyses results listed in Table 2. Al and Ca contribute to the compressive strength of geopolymers via formation of aluminosilicate gels and calcium silicate hydrates, respectively.

The effect of fly ash mass fraction in the aluminosilicate binder precursors may also be associated with the Si/Al molar ratio of the precursor blends. As the data in Table 2 indicate, Si/Al molar ratios of the precursors were 1.8 for the fly ash, and 7.8-9.2 for the slag. Si/Al values of the precursor blends used in the main experiment varied in the 2.2-3.8 range. The highest compressive strength in Table 4 was obtained at Si/Al ratio of 2.2. Published works report a rather wide range of Si/Al molar ratio that optimizes mechanical strength. For geopolymers prepared from fly ash, Wang et al. (2020) reported an optimum Si/Al ratio of 1.5. Thokchom et al. (2012) studied the effect of Si/Al ratio on the residual strength fly ash geopolymers after exposure to high temperature simulating fire. Within the Si/Al range of 1.7 to 2.2, these authors obtained the highest strength at Si/Al of 2.2. Slag-based geopolymers tend to exhibit higher optimum Si/Al ratios. Panagiotopoulou et al. (2010) reported an optimum Si/Al ratio of 3.5 for geopolymers synthesized from granulated ground blast furnace slag (GGBS). Quantification of effect of Si/Al alone in the current work was not possible since it was confounded with other variables. However, compressive strength data in Table 4 suggest that lower Si/Al tend to produce better ash-slag geopolymer strength. Nevertheless, the Si/Al range used in this work is largely in accordance with typical values reported in the literature.

Conclusions

The technical feasibility of utilizing high-magnesium ferronickel slag (FS) generated by a major ferronickel plant in Obi Island in Indonesia for geopolymer production has been proved. Due to the very high Si/Al ratio of the FS, it must be blended with coal fly ash (FA) for geopolymerization. The FS must be ground to at least approximately 70 μm (200-mesh) particle size to produce significant reactivity to activation by $NaOH/Na_2SiO_3$. Crushing strength of the FS-FA geopolymer mortars was measured in the 2.1-24.8 MPa range, with several specimens able to meet Indonesian and US industrial standards for mortar cement. Finer FS particles, higher proportion of FA, and longer heat curing period at 60°C significantly increases the geopolymer mortar compressive strength. Applying favorable values of these variables simultaneously is preferred due to synergistic interactions between them. Structural characterization by FTIR confirmed the formation of geopolymer gel phase as indicated by Si-O-Si and Si-O-Al IR absorption bands. XRD results justified the need for proper grinding of the FS to produce desirable reactivity. Overall, these results point to geopolymer production as prospective alternative pathway to alleviate the accumulation of slag in Indonesian ferronickel industry. Studies on a larger scale encompassing such aspects as process scale up, carbon capture quantification, life cycle analysis, and others shall be required to fully establish the environmental advantages of the geopolymerization of FS for the ferronickel industry in Indonesia.

Acknowledgments

This research was funded by the Research, Community Engagement, and Innovation Program (P2MI) of the Faculty of Industrial Technology, Institut Teknologi Bandung.

Compliance with ethics guidelines

The authors declare they have no conflict of interest or financial conflicts to disclose.

This article contains no studies with human or animal subjects performed by authors.

References

Al-Safi, A. A. (2021). Blast furnace slag-based geopolymer mortars cured at different conditions: modeling and optimization of compressive strength. *European Journal of Environmental and Civil Engineering*, *25*(11), 1949–1961. https://doi.org/10.1080/19648189.2019.1598502

Bewa, C. N., Tchakouté, H. K., Banenzoué, C., Cakanou, L., Mbakop, T. T., Kamseu, E., & Rüscher, C. H. (2020). Acid-based geopolymers using waste fired brick and different metakaolins as raw materials. *Applied Clay Science*, *198*, 105813. https://doi.org/10.1016/j.clay.2020.105813

Bouaissi, A., Li, L., Al Bakri Abdullah, M. M., & Bui, Q.-B. (2019). Mechanical properties and microstructure analysis of FA-GGBS-HMNS based geopolymer concrete. *Construction and Building Materials*, *210*, 198–209. https://doi.org/10.1016/j.conbuildmat.2019.03.202

Cao, R., Li, B., You, N., Zhang, Y., & Zhang, Z. (2018). Properties of alkali-activated ground granulated blast furnace slag blended with ferronickel slag. *Construction and Building Materials*, *192*, 123–132. https://doi.org/10.1016/j.conbuildmat.2018.10.112

Carreño-Gallardo, C., Tejeda-Ochoa, A., Perez-Ordonez, O. I., Ledezma-Sillas, J. E., Lardizabal-Gutierrez, D., Prieto-Gomez, C., Valenzuela-Grado, J. A., Robles Hernandez, F. C., & Herrera-Ramirez, J. M. (2018). In the CO2 emission remediation by means of alternative geopolymers as substitutes for cements. *Journal of Environmental Chemical Engineering*, *6*(4), 4878–4884. https://doi.org/10.1016/j.jece.2018.07.033

Chuewangkam, N., Kidkhunthod, P., & Pinitsoontorn, S. (2024). Direct evidence for the mechanism of early-stage geopolymerization process. *Case Studies in Construction Materials*, *21*, e03539. https://doi.org/10.1016/j.cscm.2024.e03539

Coelho, L. M., Guimarães, A. C. R., Alves Moreira, C. R. C. L., dos Santos, G. P. P., Monteiro, S. N., & da Silveira, P. H. P. M. (2024). Feasibility of Using Ferronickel Slag as a Sustainable Alternative Aggregate in Hot Mix Asphalt. *Sustainability*, *16*(19), 8642. https://doi.org/10.3390/su16198642

Detphan, S., & Chindaprasirt, P. (2009). Preparation of fly ash and rice husk ash geopolymer. *International Journal of Minerals, Metallurgy and Materials*, *16*(6), 720–726. https://doi.org/10.1016/S1674-4799(10)60019-2

Edwin, R. S., Ngii, E., Talanipa, R., Masud, F., & Sriyani, R. (2019). Effect of nickel slag as a sand replacement in strength and workability of concrete. *IOP Conference Series: Materials Science and Engineering*, *615*(1), 012014. https://doi.org/10.1088/1757-899X/615/1/012014

Falayi, T. (2019). Sustainable solidification of ferrochrome slag through geopolymerisation: a look at the effect of curing time, type of activator and liquid solid ratio. *Sustainable Environment Research*, *29*(1), 21. https://doi.org/10.1186/s42834-019-0022-7

Fansuri, H., Prasetyoko, D., Zhang, Z., & Zhang, D. (2012). The effect of sodium silicate and sodium hydroxide on the strength of aggregates made from coal fly ash using the geopolymerisation method. *Asia-Pacific Journal of Chemical Engineering*, *7*(1), 73–79. https://doi.org/10.1002/apj.493

Gomes, K. C., Carvalho, M., Diniz, D. de P., Abrantes, R. de C. C., Branco, M. A., & Carvalho Junior, P. R. O. de. (2019). Carbon emissions associated with two types of foundations: CP-II Portland cement-based composite vs. geopolymer concrete. *Matéria (Rio de Janeiro)*, *24*(4). https://doi.org/10.1590/s1517-707620190004.0850

Han, F., Zhang, H., Li, Y., & Zhang, Z. (2023). Recycling and comprehensive utilization of ferronickel slag in concrete. *Journal of Cleaner Production*, *414*, 137633. https://doi.org/10.1016/j.jclepro.2023.137633

Kaya, M., Uysal, M., Yilmaz, K., Karahan, O., & Atis, C. D. (2020). Mechanical properties of class C and F fly ash geopolymer mortars. *Journal of the Croatian Association of Civil Engineers*, *72*(04), 297–309. https://doi.org/10.14256/JCE.2421.2018

Kaze, C. R., Naghizadeh, A., Tchadjie, L., Adesina, A., Noel Yankwa Djobo, J., Deutou Nemaleu, J. G., Kamseu, E., Chinje Melo, U., & Tayeh, B. A. (2022). Lateritic soils based geopolymer materials: A review. *Construction and Building Materials*, *344*, 128157. https://doi.org/10.1016/j.conbuildmat.2022.128157

Kaze, R. C., Naghizadeh, A., Tchadjie, L., Cengiz, Ö., Kamseu, E., & Chinje, F. U. (2024). Formulation of geopolymer binder based on volcanic-scoria and clay brick wastes using rice husk ash-NaOH activator: Fresh and hardened properties. *Sustainable Chemistry and Pharmacy*, *40*, 101627. https://doi.org/10.1016/j.scp.2024.101627

Kuri, J. C., Khan, Md. N. N., & Sarker, P. K. (2021a). Fresh and hardened properties of geopolymer binder using ground high magnesium ferronickel slag with fly ash. *Construction and Building Materials*, *272*, 121877. https://doi.org/10.1016/j.conbuildmat.2020.121877

Kuri, J. C., Majhi, S., Sarker, P. K., & Mukherjee, A. (2021b). Microstructural and non-destructive investigation of the effect of high temperature exposure on ground ferronickel slag blended fly ash geopolymer mortars. *Journal of Building Engineering*, *43*, 103099. https://doi.org/10.1016/j.jobe.2021.103099

Lekshmi, S., Sudhakumar, J., & Thomas, S. (2023). Application of clay in geopolymer system: A state-of-the-art review. *Materials Today: Proceedings*. https://doi.org/10.1016/j.matpr.2023.04.083

Li, J., Sun, Z., Wang, L., Yang, X., Zhang, D., Zhang, X., & Wang, M. (2022). Properties and mechanism of high-magnesium nickel slag-fly ash based geopolymer activated by phosphoric acid. *Construction and Building Materials*, *345*, 128256. https://doi.org/10.1016/j.conbuildmat.2022.128256

Li, Q., Xu, H., Li, F., Li, P., Shen, L., & Zhai, J. (2012). Synthesis of geopolymer composites from blends of CFBC fly and bottom ashes. *Fuel*, *97*, 366–372. https://doi.org/10.1016/j.fuel.2012.02.059

Long, W.-J., Peng, J., Gu, Y., Li, J., Dong, B., Xing, F., & Fang, Y. (2021). Recycled use of municipal solid waste incinerator fly ash and ferronickel slag for eco-friendly mortar through geopolymer technology. *Journal of Cleaner Production*, *307*, 127281. https://doi.org/10.1016/j.jclepro.2021.127281

Maragkos, I., Giannopoulou, I. P., & Panias, D. (2009). Synthesis of ferronickel slag-based geopolymers. *Minerals Engineering*, *22*(2), 196–203. https://doi.org/10.1016/j.mineng.2008.07.003

DOI: 10.5614/j.eng.technol.sci.2025.57.4.1

Marczyk, J., Ziejewska, C., Pławecka, K., Bąk, A., Łach, M., Korniejenko, K., Hager, I., Mikuła, J., Lin, W.-T., & Hebda, M. (2022). Optimizing the L/S Ratio in Geopolymers for the Production of Large-Size Elements with 3D Printing Technology. *Materials*, *15*(9), 3362. https://doi.org/10.3390/ma15093362

McLellan, B. C., Williams, R. P., Lay, J., van Riessen, A., & Corder, G. D. (2011). Costs and carbon emissions for geopolymer pastes in comparison to ordinary portland cement. *Journal of Cleaner Production*, *19*(9–10), 1080–1090. https://doi.org/10.1016/j.jclepro.2011.02.010

Mishra, J., Nanda, B., Patro, S. K., & Krishna, R. S. (2024). A comprehensive review on compressive strength and microstructure properties of GGBS-based geopolymer binder systems. *Construction and Building Materials*, *417*, 135242. https://doi.org/10.1016/j.conbuildmat.2024.135242

Mustofa, M., & Pintowantoro, S. (2017). The Effect of Si/Al Ratio to Compressive Strength and Water Absorption of Ferronickel Slag-based Geopolymer. *IPTEK Journal of Proceedings Series*, *0*(2), 167. https://doi.org/10.12962/j23546026.y2017i2.2334

Ng, C., Alengaram, U. J., Wong, L. S., Mo, K. H., Jumaat, M. Z., & Ramesh, S. (2018). A review on microstructural study and compressive strength of geopolymer mortar, paste and concrete. *Construction and Building Materials*, *186*, 550–576. https://doi.org/10.1016/j.conbuildmat.2018.07.075

Nguyen, Q. D., & Castel, A. (2023). Developing Geopolymer Concrete by Using Ferronickel Slag and Ground-Granulated Blast-Furnace Slag. *Ceramics*, *6*(3), 1861–1878. https://doi.org/10.3390/ceramics6030114

Niş, A. (2019). Compressive strength variation of alkali activated fly ash/slag concrete with different NaOH concentrations and sodium silicate to sodium hydroxide ratios. *Journal of Sustainable Construction Materials and Technologies*, *4*(2), 351–360. https://doi.org/10.29187/jscmt.2019.39

Panagiotopoulou, C., Kakali, G., Tsivilis, S., Perraki, T., & Perraki, M. (2010). Synthesis and Characterisation of Slag Based Geopolymers. *Materials Science Forum*, *636–637*, 155–160. https://doi.org/10.4028/www.scientific.net/MSF.636-637.155

Petrakis, E., Karmali, V., & Komnitsas, K. (2019). Effect of Particle Size on Alkali-Activation of Slag. *International Journal of Materials and Metallurgical Engineering*, *13*(9), 471–474.

Rosas-Casarez, C., Arredondo-Rea, S., Cruz-Enríquez, A., Corral-Higuera, R., Pellegrini-Cervantes, M., Gómez-Soberón, J., & Medina-Serna, T. (2018). Influence of Size Reduction of Fly Ash Particles by Grinding on the Chemical Properties of Geopolymers. *Applied Sciences*, *8*(3), 365. https://doi.org/10.3390/app8030365

Samantasinghar, S., & Singh, S. P. (2019). Fresh and Hardened Properties of Fly Ash–Slag Blended Geopolymer Paste and Mortar. *International Journal of Concrete Structures and Materials*, *13*(1), 47. https://doi.org/10.1186/s40069-019-0360-1

Shang, W., Peng, Z., Xu, F., Tang, H., Rao, M., Li, G., & Jiang, T. (2021). Preparation of enstatite-spinel based glass-ceramics by co-utilization of ferronickel slag and coal fly ash. *Ceramics International*, *47*(20), 29400–29409. https://doi.org/10.1016/j.ceramint.2021.07.108

Simão, L., Fernandes, E., Hotza, D., Ribeiro, M. J., Montedo, O. R. K., & Raupp-Pereira, F. (2021). Controlling efflorescence in geopolymers: A new approach. *Case Studies in Construction Materials*, *15*, e00740. https://doi.org/10.1016/j.cscm.2021.e00740

Tao, J.-C., Wang, X.-Z., Yao, B., Pei, W.-W., Jiren, G., He, W.-Q., & Li, L. (2025). Comparison of rheology and durability of geopolymer and Portland cement concrete at the same strength levels. *Construction and Building Materials*, *461*, 139958. https://doi.org/10.1016/j.conbuildmat.2025.139958

Tchakouté, H. K., & Rüscher, C. H. (2017). Mechanical and microstructural properties of metakaolin-based geopolymer cements from sodium waterglass and phosphoric acid solution as hardeners: A comparative study. *Applied Clay Science*, *140*, 81–87. https://doi.org/10.1016/j.clay.2017.02.002

Thokchom, S., Mandal, K. Kr., & Ghosh, S. (2012). Effect of Si/Al Ratio on Performance of Fly Ash Geopolymers at Elevated Temperature. *Arabian Journal for Science and Engineering*, *37*(4), 977–989. https://doi.org/10.1007/s13369-012-0230-5

Tian, Q., Pan, Y., Bai, Y., Yao, S., & Sun, S. (2022). A Bibliometric Analysis of Research Progress and Trends on Fly Ash-Based Geopolymer. *Materials*, *15*(14), 4777. https://doi.org/10.3390/ma15144777

U.S. Geological Survey. (2024). *Mineral commodity summaries 2024*. https://doi.org/10.3133/mcs2024

Vásquez, A., Cárdenas, V., Robayo, R. A., & de Gutiérrez, R. M. (2016). Geopolymer based on concrete demolition waste. *Advanced Powder Technology*, *27*(4), 1173–1179. https://doi.org/10.1016/j.apt.2016.03.029

Wang, Y., Hu, Y., He, X., Su, Y., Strnadel, B., & Miao, W. (2023). Hydration and compressive strength of supersulfated cement with low-activity high alumina ferronickel slag. *Cement and Concrete Composites*, *136*, 104892. https://doi.org/10.1016/j.cemconcomp.2022.104892

Wang, Y., Liu, X., Zhang, W., Li, Z., Zhang, Y., Li, Y., & Ren, Y. (2020). Effects of Si/Al ratio on the efflorescence and properties of fly ash based geopolymer. *Journal of Cleaner Production*, *244*, 118852. https://doi.org/10.1016/j.jclepro.2019.118852

Wardhono, A. (2018). Comparison Study of Class F and Class C Fly Ashes as Cement Replacement Material on Strength Development of Non-Cement Mortar. *IOP Conference Series: Materials Science and Engineering*, *288*, 012019. https://doi.org/10.1088/1757-899X/288/1/012019

Wu, Y., Wang, M., Sun, Z., & Zhang, D. (2024). High temperature performance of high magnesium nickel slag based geopolymers with different P/Al molar ratios prepared by acidic activator. *Case Studies in Construction Materials*, *20*, e03275. https://doi.org/10.1016/j.cscm.2024.e03275

Xu, Z., Yue, J., Pang, G., Li, R., Zhang, P., & Xu, S. (2021). Influence of the Activator Concentration and Solid/Liquid Ratio on the Strength and Shrinkage Characteristics of Alkali-Activated Slag Geopolymer Pastes. *Advances in Civil Engineering*, *2021*, 1–11. https://doi.org/10.1155/2021/6631316

Yang, T., Yao, X., & Zhang, Z. (2014). Geopolymer prepared with high-magnesium nickel slag: Characterization of properties and microstructure. *Construction and Building Materials*, *59*, 188–194. https://doi.org/10.1016/j.conbuildmat.2014.01.038

Yang, T., Wu, Q., Zhu, H., & Zhang, Z. (2017). Geopolymer with improved thermal stability by incorporating high-magnesium nickel slag. *Construction and Building Materials*, *155*, 475–484. https://doi.org/10.1016/j.conbuildmat.2017.08.081

Yanning, S., Qiao, H., Qiong, F., Chao, W., & Jianghua, Z. (2024). Application of metallurgical ferronickel slag in building materials: A review. *Journal of Building Engineering*, *96*, 110632. https://doi.org/10.1016/j.jobe.2024.110632

Zulhan, Z., & Agustina, N. (2021). A novel utilization of ferronickel slag as a source of magnesium metal and ferroalloy production. *Journal of Cleaner Production*, *292*, 125307. https://doi.org/10.1016/j.jclepro.2020.125307.

Manuscript Received: 8 November 2024
Revised Manuscript Received: 22 March 2025
Accepted Manuscript: 20 May 2025